Remote Sensing of Environment 183 (2016) 170–185

Contents lists available at ScienceDirect

Remote Sensing of Environment

journal homepage: www.elsevier.com/locate/rse

Detailed dynamic land cover mapping of Chile: Accuracy improvement by integrating multi-temporal data

Yuanyuan Zhao [a], Duole Feng [a], Le Yu [a], Xiaoyi Wang [b,c], Yanlei Chen [c], Yuqi Bai [a], H. Jaime Hernández [d], Mauricio Galleguillos [e,h], Cristian Estades [f], Gregory S. Biging [c], John D. Radke [g], Peng Gong [a,b,c,*]

[a] Ministry of Education Key Laboratory for Earth System Modelling, Centre for Earth System Science, Tsinghua University, Beijing 100084, China
[b] State Key Laboratory of Remote Sensing Science, Jointly Sponsored by Institute of Remote Sensing and Digital Earth, Chinese Academy of Sciences, and Beijing Normal University, Beijing 100101, China
[c] Department of Environmental Science, Policy, and Management, UC Berkeley, Berkeley, CA 94720, USA
[d] Geomatics and Landscape Ecology Lab, Forestry and Nature Conservation Faculty, University of Chile, Santiago, Chile
[e] Department of Environmental Sciences, Faculty of Agronomic Sciences, University of Chile, Santiago, Chile
[f] Wildlife Ecology Lab, Forestry and Nature Conservation Faculty, University of Chile, Santiago, Chile
[g] Department of Landscape Architecture and Environmental Planning, UC Berkeley, Berkeley, CA 94720, USA
[h] Center for Climate and Resilience Research (CR)2, University of Chile, Santiago, Chile

ARTICLE INFO

Article history:
Received 22 August 2015
Received in revised form 11 May 2016
Accepted 23 May 2016
Available online 6 June 2016

Keywords:
Land cover mapping
Landsat
Seasonal dynamics
Biodiversity
30 m

ABSTRACT

Stretching over 4300 km north to south, Chile is a special country with complicated landscapes and rich biodiversity. Accurate and timely updated land cover map of Chile in detailed classification categories is highly demanded for many applications. A conclusive land cover map integrated from multi-seasonal mapping results and a seasonal dynamic map series were produced using Landsat 8 imagery mainly acquired in 2013 and 2014, supplemented by MODIS Enhanced Vegetation Index data, high resolution imagery on Google Earth, and Shuttle Radar Topography Mission DEM data. The overall accuracy is 80% for the integrated map at level 1 and 73% for level 2 based on independent validation data. Accuracies for seasonal map series were also assessed, which is around 70% for each season, greatly improved by integrated use of seasonal information. The importance of growing season imagery was proved in our analysis. The analysis of the spatial variation of accuracies among various ecoregions indicates that the accuracy for land cover mapping decreases gradually from central Chile to both north and south. More mapping efforts for those ecoregions are needed. In addition, the training dataset includes sample points spatially distributed in the whole country, temporally distributed throughout the year, and categorically encompassing all land cover types. This training dataset constitutes a universal sample set allowing us to map land cover from any Landsat 8 image acquired in Chile without additional ad hoc training sample collection.

1. Introduction

Land cover information plays a key role in many Earth system studies (Yang et al., 2013). It is an important input to Earth system models (Dai et al., 2003; Jung, Henkel, Herold, & Churkina, 2006; Liu, Chen, Cihlar, & Park, 1997) or habitat models (Liang et al., 2010; Özesmi & Mitsch, 1997; Pearson, Dawson, & Liu, 2004; Yu, Shi, & Gong, 2015). It is also essential for natural resources planning and management (Gong, 2012; LaFontaine, Hay, Viger, Regan, & Markstrom, 2015; Pauleit & Duhme, 2000; Zhong, Gong, & Biging, 2012). Although a large number of efforts have been made to map land cover at various spatial scales, the quality of land cover maps are hardly satisfactory to meet the needs of diverse user communities (Yu et al., 2014a). A large gap in land cover mapping is the shortage of land cover maps at the national scale for many countries in the world. Global land cover maps cannot fully fill this gap because their land cover categories are usually designed for specific global applications. Given the considerably improved availability of medium resolution satellite data and data processing capabilities, a critical task in producing useful land cover maps for a particular country is adopting a land cover classification scheme developed with the participation of users in that country. Chile is such a country that does not have a comprehensive land cover map at medium spatial resolution. This study describes our national land cover mapping effort for Chile.

Bounded by the Pacific on the west, the Andes on the east and the Atacama Desert in the north, Chile is a virtual continent island stretching over 4300 km north to south with rich biodiversity. Notably

* Corresponding author at: Ministry of Education Key Laboratory for Earth System Modelling, Centre for Earth System Science, Tsinghua University, Beijing 100084, China.
E-mail address: penggong@tsinghua.edu.cn (P. Gong).

http://dx.doi.org/10.1016/j.rse.2016.05.016
0034-4257/

Table 1
Regional land cover products covering the entire Chile.

Product name	Data time	Resolution	Sensor	Scheme	Reference
UMD SA	1987–1983	1 km	AVHRR	16 classes	Townshend et al. (1987)
LBA-ECO	1987–1991	1 km	AVHRR	39 classes	Stone et al. (1994)
JRC SA	1995–2000	1 km	ATSR, VGT, OLS	10 classes (L1)	Eva et al. (2004)
SERENA	2008	500 m	MODIS	22 classes	Blanco et al. (2013)
MERISAM2009	2009–2010	300 m	MERIS	9 classes	Hojas Gascon et al. (2012)
USGS SA	2010	30 m	TM, ETM +	5 classes	Giri & Long (2014)

a high rate (about 45%) of the species are endemic, which can be attributed to its isolation (Squeo et al., 2012). The climate regions vary from tropical desert and semi-desert in the north, Mediterranean in the middle, temperate oceanic and sub-polar oceanic in the south. Under the effects of both climate and topography, the natural vegetation types are highly diverse. In the north lies the driest Atacama Desert, with almost no vegetation at its heart, low scrub vegetation towards the Andes and sparse shrub called the "Lomas" towards the coast, highly depending on coastal fog and humidity. After a transitional zone of matorral (shrubs) and savannas southward, the vegetation changes to Mediterranean sclerophyll woodlands and high shrubs. With the remarkable presence of the typical Araucanía forests and krummholz, the deciduous forests in central Chile transit towards temperate rain forests with high precipitation levels. For the fjords and islands in the far south, it becomes moorlands or icefields and oceanic forests reappear (Moreira-Muñoz, 2011). Chile's complicated landscape and diverse vegetation requires a monitoring approach that uses multi-temporal imagery of sufficient spatial resolution to capture important phases in the vegetation dynamics of the landscape. For example, a series of seasonal dynamic land cover map of high resolution could even capture the moment when geophytes and annuals sprout from the seemingly bare land.

Since the 1950s, the land cover type of southern-central Chile is dominated by fast-growing commercial plantations, mainly including radiate pine and eucalyptus (Toro & Gessel, 1999). Forests change mainly occurs in this region, with a loss of more than 1 million hectares and a concurrent gain of about the same area from 2001 to 2013, according to Global Forest Watch (an online platform for the public to help monitor forest change, http://www.globalforestwatch.org/), reflecting the rapid rotations of logging and replantation of trees. With the log exports being reduced, harvested wood is processed into primary and secondary products, including paper, pulp, sawnwood, engineered wood products and furniture, and 75% of the product is exported mainly to the United States, Japan and China (Cartwright & Gaston, 2002). The carbon

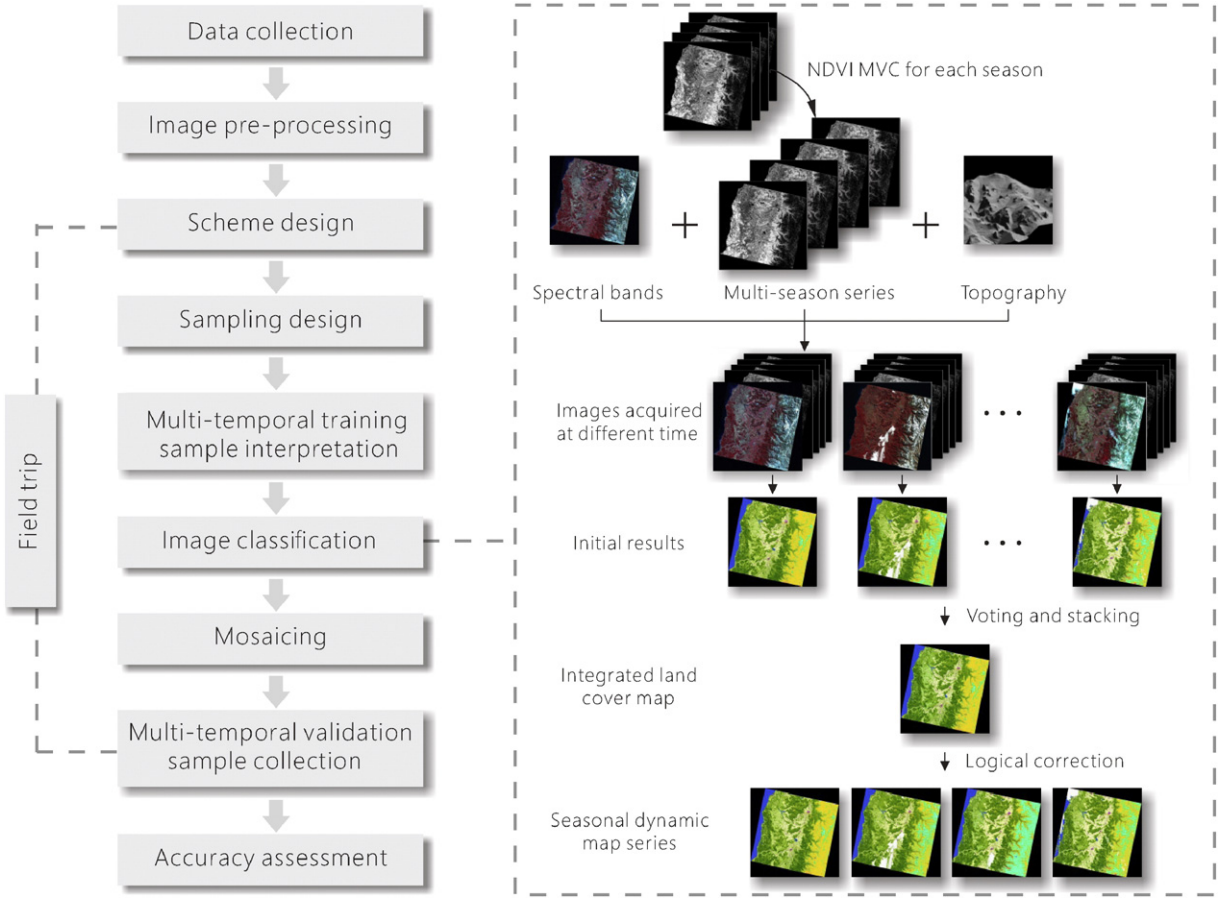

Fig. 1. Flowchart of the Chilean land cover mapping process.

Table 2
Land cover classes in the classification scheme used in this study.

Level 1	Level 2	Level 3
100 croplands	110 rice fields	
	120 greenhouse farming	
	130 other croplands	
	140 orchards	
	150 bare croplands/fallow	
200 forests	210 natural broadleaf	211 primary
		212 secondary
	220 natural conifer	221 primary
		222 secondary
	230 natural mixed	
	240 broadleaf plantations	241 old plantations
		242 clearcuts
	250 conifer plantations	251 old plantations
		252 clearcuts
300 grasslands	310 pastures	
	320 other grasslands	
	330 withered grasslands	
400 shrublands	410 shrublands	
	420 shrubs and sparse trees mosaic	
	430 succulents	
	440 shrub plantations	
	450 withered shrublands	
500 wetlands	510 marshlands	
	520 mudflats	
	530 other wetlands	
600 water bodies	610 lakes	
	620 reservoirs/ponds	
	630 Rivers	
	640 ocean	
800 impervious surfaces		
900 barren lands	910 dry salt flats	
	920 sandy areas	
	930 bare exposed rocks	931 rocks
		932 gravels
1000 snow and ice	1010 snow	
	1020 ice	
1200 clouds		

sequestration dynamics and carbon sink potential of plantations are also of wide interest (Espinosa, Acuña, Cancino, Muñoz, & Perry, 2005), which would be greatly facilitated by a long-time series of high resolution plantation maps. Another important problem related to plantation is the concerns about ecosystem services. The diverse native forests were replaced by single species, affecting the habitat and biodiversity, water regulation, and soil fertility. Having a map of the plantation and native forests makes it possible for researchers to study the balance of economic benefits and ecosystem services (Panayotou & Ashton, 1992). Since additional stress caused by plantations comes from insect outbreaks (Lanfranco & Dungey, 2001), risk and vulnerability analysis is necessary, which needs the pattern of plantation and native forests as a basic input.

Land cover mapping has long been focused in Europe, North America, and even Asia, resulting in better products over many of these areas. Except for global land cover products, a few regional land cover products were developed for South America (summarized in Table 1). The first generation of specialized land cover product for South America was 1 km resolution using AVHRR NDVI time series acquired in April 1982 to March 1983 (Townshend, Justice, & Kalb, 1987), followed by another 1 km resolution product generated by visual interpretation covering 1987 to 1991 (Stone, Schlesinger, Houghton, & Woodwell, 1994), 1 km resolution product mainly derived by Joint Research Centre of the European Commission for 2000 (Eva et al., 2004), 300 m resolution MERISAM2009 for 2009 (Hojas Gascon, Eva, Gobron, Simonetti, & Fritz, 2012) and 500 m resolution SERENA for 2008 (Blanco et al., 2013). The latest product for South America was 30 m resolution derived by USGS for 2010 using mainly Landsat 5 TM and Landsat 7 ETM + images (Giri & Long, 2014). They only used the Landsat images of growing season, but we believe there is more information we can extract from the images outside the growing season. They mapped 5 classes, including trees, open water, barren, perennial snow/ice and other vegetation, but the classification scheme lacks details for many thematic applications. The 5 classes were conclusive land cover classes, but for many applications we need seasonal dynamics of the land cover classes. For validation, they used 55 of the 500 validation sites (Olofsson et al., 2012) located in South America, and there are only 4 sites in Chile, and 3 of them are distributed in Central Chile, so the Chile part of the product has not been fully validated. There are also a few local maps focusing on specific scope of applications, for example, mapping a part of Araucanía Region to study native forest loss and turnover (Altamirano et al., 2013), mapping a part of Maule and Bío-Bío regions to study plantation change (Nahuelhual, Carmona, Lara, Echeverra, & González, 2012), and mapping an area in the Valparaíso, O'Higgins and Metropolitan regions to study the transformation from Mediterranean vegetation to intensive cultural landscapes (Schulz, Cayuela, Echeverria, Salas, & Benayas, 2010).

Temporal information has long been one of the most important information source for medium resolution land cover mapping (Arvor, Jonathan, Meirelles, Dubreuil, & Durieux, 2011; Friedl et al., 2010; Hansen, DeFries, Townshend, & Sohlberg, 2000; Tucker, Townshend, & Goff, 1985). With better data availability of multi-temporal high resolution images, the use of more than one image for a single year was proved useful on improving mapping accuracy. The most effective application of multi-temporal images is the croplands mapping (Brisco & Brown, 1995; Lo, Scarpace, & Lillesand, 1986; Peña & Brenning, 2015; Zhong, Gong, & Biging, 2014). Besides, multi-temporal images were also useful in mapping grasslands (Guerschman, Paruelo, Bella, Giallorenzi, & Pacin, 2003; Henebry, 1993), forests (Fagan et al., 2015; Wolter, Mladenoff, Host, & Crow, 1995) and wetlands (Dong et al., 2014; Munro & Touron, 1997). Most of these studies chose two to six images of different time to combine in the feature set (Homer et al., 2007; Senf, Leitão, Pflugmacher, van der Linden, & Hostert, 2015; Schriever & Congalton, 1995; Zhu, Woodcock, Rogan, & Kellndorfer, 2012), but the problem is we cannot ensure the same number of high quality images covering different path/row locations for large scale land cover mapping. Some researchers extracted some metrics from long or short time series (for example, median and mean of three earliest and latest observations ordered by date) and added them to the feature set (Potapov et al., 2015). However, in this way we can end up with same data structure for classification inputs, but we may have information loss in this process. This study selected a light-weight feature set, and tried our best to make full use of our multi-seasonal training sample set, because improving training sample is the most direct way to improve classification performance. A common model was built for the classification of every image we have, no matter where it was, when it was acquired or how many images for each season we have for the same area. Additionally, the study areas in most of the previous dynamic land cover mapping studies that dealt with both conclusive land cover types and seasonal land cover types were limited to regional or smaller scales (Dronova, Gong, Wang, & Zhong, 2015; Hess, Melack, Novo, Barbosa, & Gastil, 2003; Sun, Zhao, Gong, Ma, & Dai, 2014; Wang et al., 2015). This study is the first attempt to derive a dynamic land cover product at national scale to depict the seasonal land cover variation of Chile, a country stretching over 4300 km north to south with different climate zones and topographic conditions.

In this paper, we described a detailed land cover database of Chile for 2014, including a conclusive land cover map and a series of seasonal dynamic land cover maps. The land cover maps were validated using an independent sample dataset and the accuracies were reported. The spatial variation of accuracy among different ecoregions was analyzed as well.

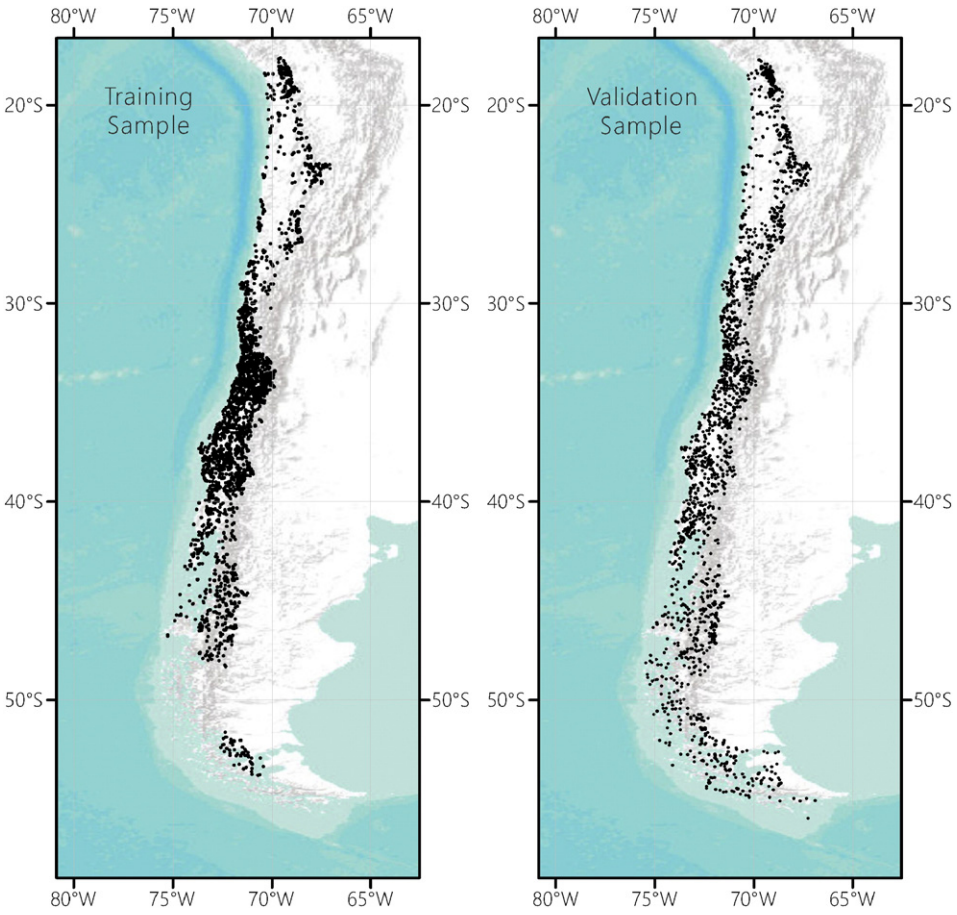

Fig. 2. The spatial distribution of training (left) and validation (right) sample set.

2. Methods

Fig. 1 illustrates an overview of the process in this mapping project, including the data collection and pre-processing, classification scheme and sampling design, training sample collection, classification, and accuracy assessment.

2.1. Data collection and pre-processing

A total of 1605 images acquired by Landsat 8 Operational Land Imager (OLI) for 2013 and 2014 were downloaded from the USGS archives. Normally, there are several scenes for each season (i.e., spring, summer, autumn and winter in astronomic definition) at a certain Worldwide Reference System 2 (WRS2) path/row location, but images with more than 20% cloud cover were dropped from the mapping dataset to reduce the computation workload, resulting in insufficient data for some specific seasons over certain locations. To ensure at least one scene for each season at each path/row location, three scenes with the least cloud cover were used as supplements, including some newly acquired in 2015. All these scenes were then radiometric calibrated and atmospheric corrected using the Global Mapper (GM) software package developed by our group (Gong et al., 2013). To support the sampling, interpretation, and post-classification analysis, ancillary data includes the time series of a 16-day composite of Moderate Resolution Imaging Spectroradiometer (MODIS) Enhanced Vegetation Index (EVI) for the period of the years 2011 to 2014, a vector land cover database constructed by Chilean Forestry Services, and high resolution imagery on Google Earth (Zhao et al., 2014). 30 m resolution Shuttle Radar Topography Mission (SRTM) DEM was used as well, due to the complex topography in Chile.

2.2. Classification scheme design and sample collection

The classification scheme was designed with Chilean geographers and biodiversity researchers, mainly based on the scheme used in the FROM-GLC project (Gong et al., 2013). Some classes were refined to several subclasses, driven by the application demands on biodiversity conservation, resource planning and land surface modelling. This classification scheme includes 10 classes at level 1, 30 level 2 and 35 level 3 classes (see Table 2) which are potentially separable with available data. Most of the classes could be defined using the Land Cover Classification System (LCCS) method, which is a common language for description and characterization of land cover features, for better comparison and correlation of land cover classes in different classification schemes (Di Gregorio, 2005). With additional information on canopy coverage and height, the classes in this scheme can be cross-walked better to others, such as FAO land cover classification system and the IGBP land cover classification system. These detailed classes enable the land cover maps to be used as fundamental data in applications of different fields. For example, to provide adequate information for forest management and protection, plantation and natural forest were separated. The subclasses of leaf type can be used for land surface parameterization for models. The differentiation of herbaceous croplands, orchard, and pasture made it possible to conduct further agricultural analysis, such as agricultural mode and its impact on biogeochemical cycles.

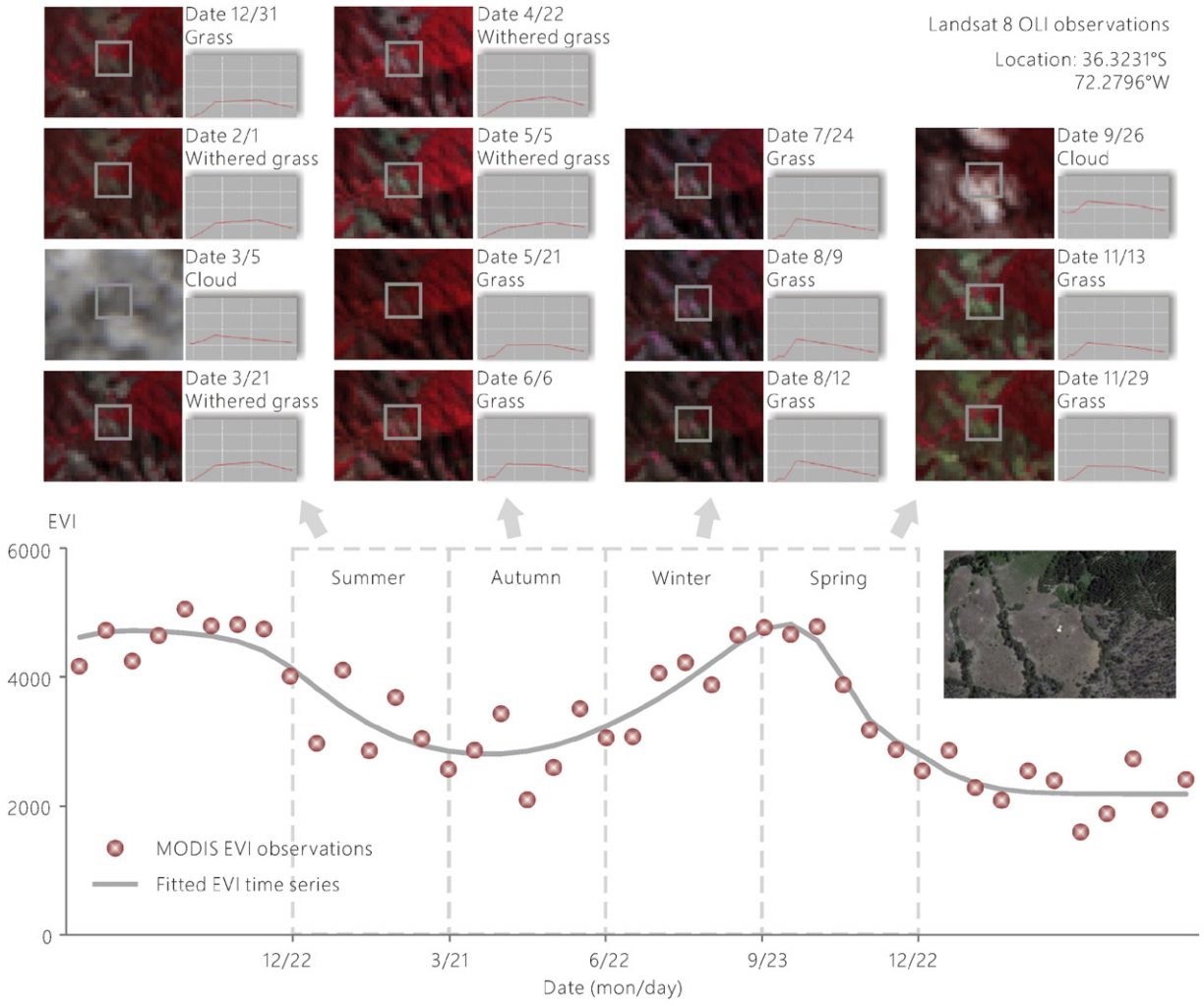

Fig. 3. Multi-temporal Landsat image interpretation. Multi-temporal Landsat images were shown and the curves next to each window of Landsat image are the spectral profiles of the center pixel. The horizontal axis represents the wavelength of each spectral band, and the vertical axis represents the reflectance. The supporting data of MODIS EVI observations and high resolution image on Google Earth for the same location were also presented.

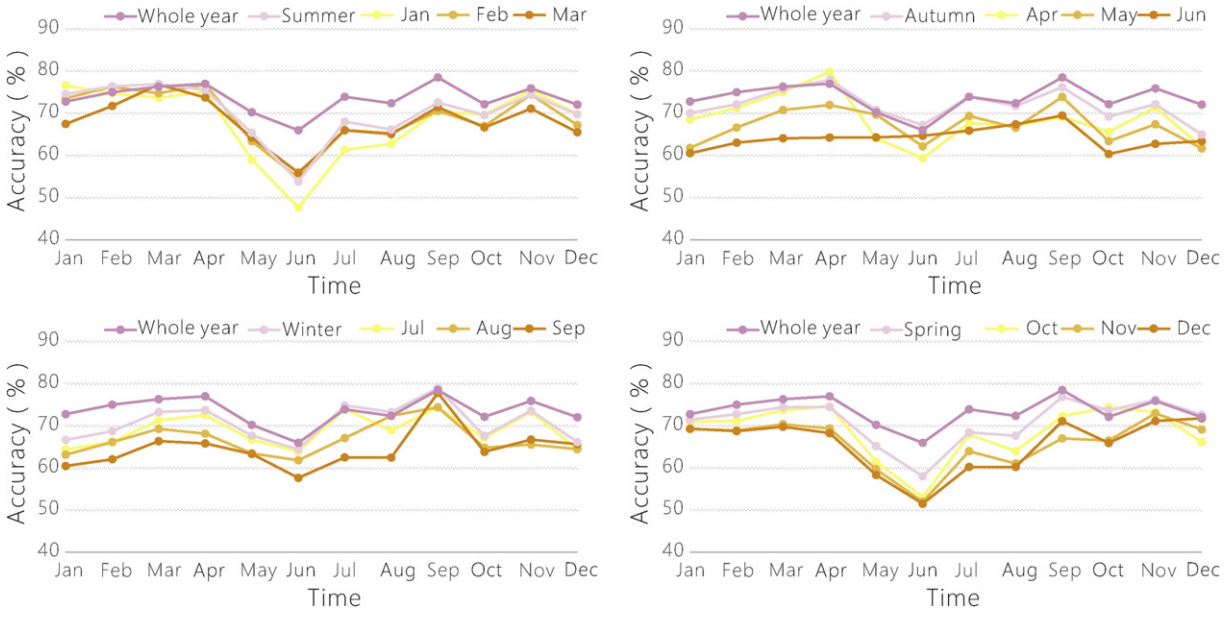

Fig. 4. Classification accuracies of the image acquired in each month by the model trained by training samples of each month, each season, or the whole year (feature set only includes spectral bands of single image).

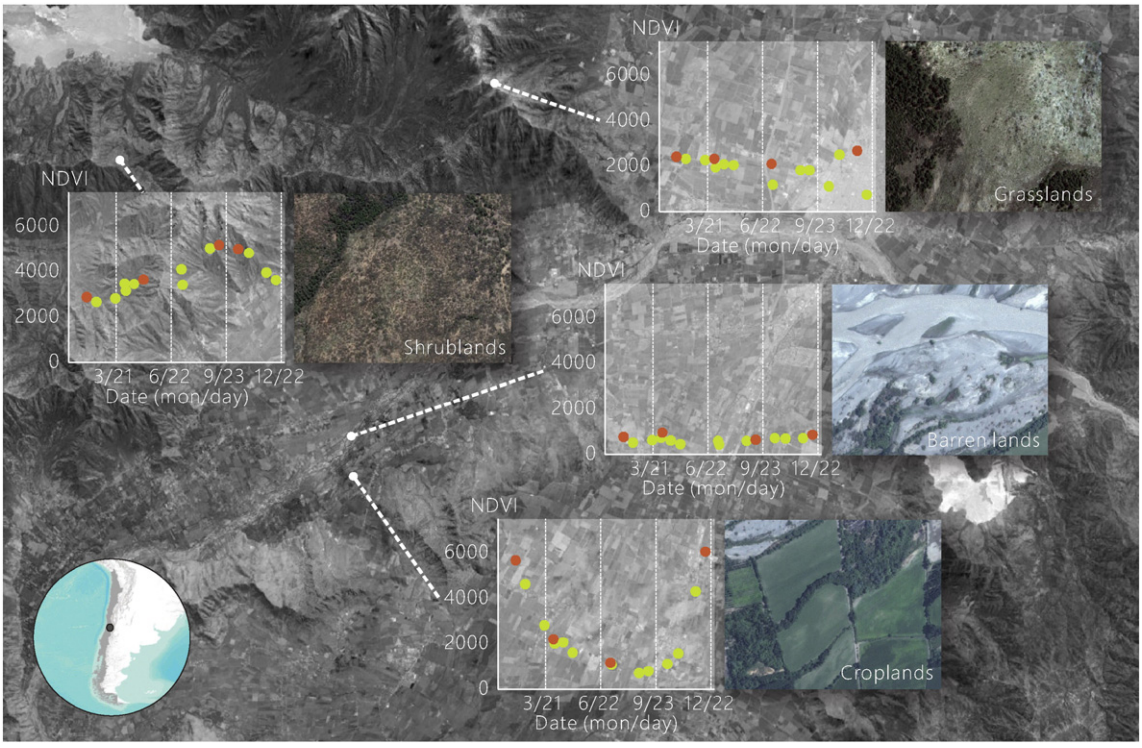

Fig. 5. Examples showing the differences of NDVI time series derived from multi-temporal Landsat images among land cover types including shrublands, grasslands, barren lands and croplands. The green dots are NDVI observations of multi-temporal Landsat images, and the orange dots are MVC results for each season.

The training and validation datasets were sampled independently using stratified random sampling based on the prior knowledge provided by the Chilean Forestry Services Database, which contains generalized polygons, labelled with major land cover classes. The spatial distribution of training and validation sample set are presented in Fig. 2. Since the training sample set should be relatively homogeneous,

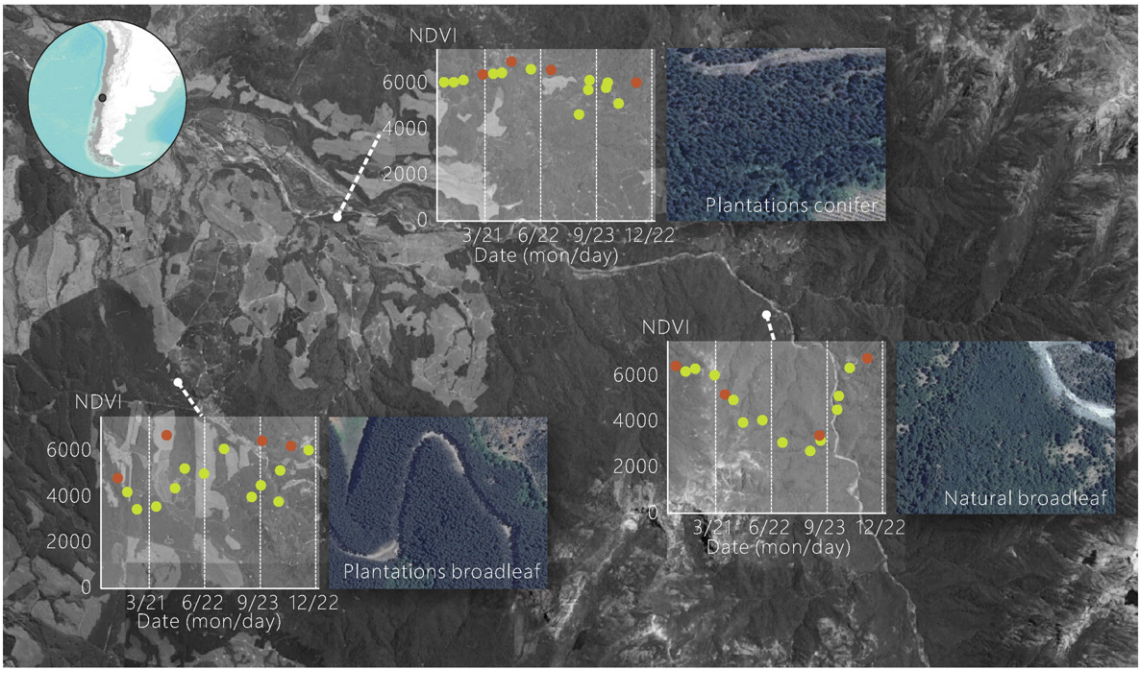

Fig. 6. Examples showing the differences of NDVI time series derived from multi-temporal Landsat images among land cover types including natural forests and plantations. The green dots are NDVI observations of multi-temporal Landsat images, and the orange dots are MVC results for each season.

comprehensive and representative, 160 by 160 pixel image blocks of all phenological stages for all 2957 sampled "seed location" were extracted for manual interpretation. One to five training sites of the land cover type labelled for the polygon in Chilean Forestry Services Database were selected from each image block and labelled with a time series of land cover class according to multi-temporal Landsat images. Fig. 3 demonstrates the multi-temporal interpretation of a training sample in central Chile as an example. Dominated by subtropical high pressure during summer, the precipitation is limited resulting in the seasonal alternation of grassland and withered grassland. The curves next to each window of Landsat image are the spectral profiles of the center pixel. We can see the changing shape of the spectral profiles through multi-temporal observations. For example, from Dec. 31 to May 5, the spectral profiles present a wilting process of green vegetation by the decreasing red absorption and near-infrared reflection, followed by a green-up process after May 5 showing an increasing red absorption and near-infrared reflection. The land cover type was interpreted dynamically for multi-temporal Landsat images, and interpretations for different time were all recorded in the sample set. The interpretation was also supported by MODIS EVI time series, high resolution imagery, historical imagery, street views and photos on Google Earth to lower uncertainty. Beside the acquisition time of the interpreted Landsat image (DOY and year) and the spatial size which is homogeneous around the sample (1, 3, 8 or 17 pixels of 30 m), the disturbance of thin clouds, cloud shadows, relief shadows and snow background are also marked in each record of interpretation. As a result, we collected 4107 basic locations for training. For each location we interpreted multi-temporal Landsat images, and got 40,162 temporal interpretation records (with an average of 10 different temporal interpretation records for each location). Each interpretation record can be spatially expanded depending on the spatial size which is homogeneous around the sample location (1, 3, 8 or 17 pixels of 30 m). Finally, we got 1,227,467 pixels of 30 m in the training dataset. The validation sample set was collected two ways: manual interpretation and field visitation. Unlike training samples which were manually selected in the stratified sampling blocks, validation sample sites were randomly generated by stratified sampling to ensure an objective accuracy assessment. To get a better sense of local land cover and collect more accurate ground-based observations, accumulatively 4000 km of field trips were taken as far north as Atacama and as far south as Los Lagos. Approximately one thousand field points were carefully collected for validation.

2.3. Classification strategy

Random Forest was chosen in this study, because it is an efficient supervised classifier with top-class performance among many machine learning methods (Gong et al., 2013). Random Forest is an ensemble machine learning method that fits a multitude of decision trees using subsets of training samples and integrates predictions of the individual trees to improve classification accuracy and control over-fitting. The parameters for the classifier were determined from preliminary experiments. For example, we chose 100 as the number of trees in the forest, which achieved a good balance between prediction performance and cost in computation time. With corresponding land cover labels, all spectral profiles extracted from images acquired at different times for the training sites can be used to enrich the spectral diversity of the training dataset. For the same purpose, training samples can be spatially expanded surrounding the center of sample locations, according to their homogeneity.

In the past, for land cover mapping at larger scale, images were usually classified using a model trained by training samples of similar time and space, namely Spatial Temporal Sample Search (STS) approach (Gong et al., 2013). Unexpectedly, a common classification model for global land cover mapping was proved to have better accuracy (Yu et al., 2014b). Therefore, in this study we want to build a spatial and temporal common model which is suitable for the classification of any Landsat scene. In order to test the effectiveness of the combination of multi-temporal training samples, we trained the model with only samples of each month and each season respectively, and used each model to classify all validation samples. The accuracies were compared with the accuracy we got when the model was trained by the combination of multi-temporal training samples. The feature set was simplified to only spectral bands of single image in this experiment. According to the results (shown in Fig. 4), model trained by the combination of multi-temporal sample set performed better than the ones trained by the sample set of single season or single month. Generally the model

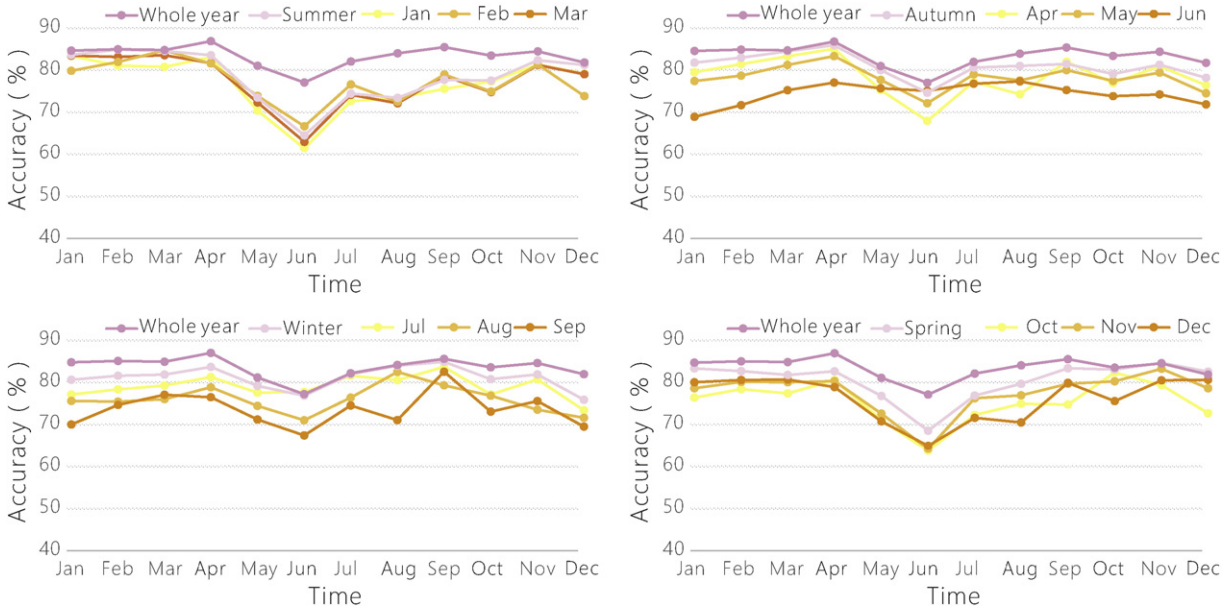

Fig. 7. Classification accuracies of the image acquired in each month by the model trained by training samples of each month, each season, or the whole year (new feature combination includes multi-temporal NDVI series).

trained by the sample set of each month worked best on the classification of images acquired around the same time, while its performance was weak if the time gap is large. This experiment results clearly show the advantage of the design of using multi-temporal training sample set in this study.

Features selected for classification include not only spectral data and NDVI (Normalized Difference Vegetation Index) as well as NDWI (Normalized Difference Water Index) calculated from the Landsat scene for classification, but also a multi-season NDVI series derived from all Landsat images acquired on different dates for the

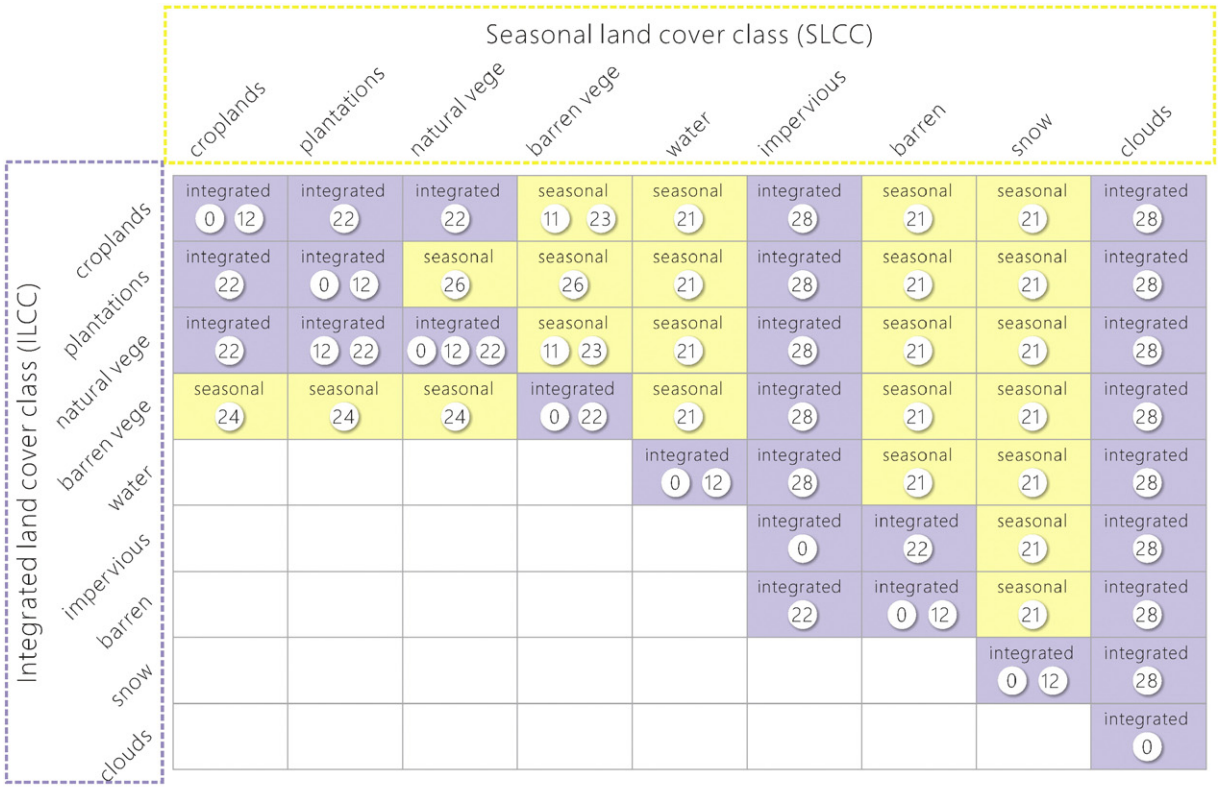

Legend

integrated 0 — The original seasonal class or the integrated class was used for the corrected seasonal map / The uncertainty code for the corrected seasonal map

0 If ILCC and SLCC are the same, nothing was changed.

11 If ILCC and SLCC belong to the same level 1 class, and SLCC could possibly occur in the seasonal variation of ILCC, SLCC was kept.

12 If ILCC and SLCC belong to the same level 1 class, and are very similar, only level 2 of SLCC was changed.

21 If ILCC and SLCC belong to different level 1 classes, but SLCC could possibly occur in the seasonal variation of ILCC, SLCC was kept.

22 If ILCC and SLCC belong to different level 1 classes, but are quite similar, both levels of SLCC were changed.

23 If ILCC and SLCC belong to different level 1 classes, but SLCC is quite similar to class X which could possibly occur in the seasonal variation of ILCC, SLCC was modified to X.

24 If ILCC and SLCC belong to different level 1 classes, but they are not similar, SLCC was kept.

26 If ILCC and SLCC belong to different level 1 classes, but SLCC would possibly be affected by plantation rotation, SLCC was kept.

28 If SLCC is cloud or impervious surface, both levels of SLCC were changed.

Note: 'natural vege' stands for natural vegetation, including natural forests, grasslands and shrublands. 'barren vege' stands for the special phenological stage of vegetation which is not green, including bare croplands, withered grasslands and withered shrublands

Fig. 8. The logical rules for the correction of seasonal land cover map according to the integrated map.

same location to help differentiate land cover classes with seasonal variation. Synthetic data was generated by NDVI MVC (maximum value composite) algorithm for each season to minimize cloud contamination, shadow effects, aerosol and water vapor effects (Holben, 1986). In the calculation of the multi-season NDVI MVC series for training samples, if there are several interpretation records (different DOYs) in the same season, records without any disturbance would be used with high priority. Two groups of examples were given to show the differences of NDVI time series derived from multi-temporal Landsat images among different land cover types. The samples in each group are very close to each other, sharing similar climate conditions, but their NDVI time series are different due to the land cover differences. In Fig. 5, the NDVI of shrubland begins to increase in autumn and reaches to the peak in winter. The example of grasslands is on the mountain ridge, and the NDVI maintained at about 2000 throughout the year. The example of barren lands is on the flood plain of a river, with NDVI below 1000 continuously. The example of croplands starts growing when spring comes, peaks in summer and is harvested in autumn. The spectral data maybe similar for two land cover types in one season, but they have different signatures of NDVI time series. Similarly, Fig. 6 shows the difference clearly among three forest types in this area. Conifer plantations have high and stable NDVI for all seasons, while broadleaf plantations have lower NDVI in dry summer. Natural broadleaf forests turn yellow in winter, so their NDVI drop to the lowest. Even though the calculation of MVC results in loss of information, it helps to eliminate the disturbance of clouds, and the temporal pattern is kept basically. We tested many combinations of features, our final selected one achieved the best accuracies (shown in Fig. 7), mainly owing to the multi-temporal NDVI series. The average accuracy of all months without the multi-temporal NDVI series in the feature set was 73.8%, but this number rose to 83.5% using final selected feature set.

All Landsat images were classified, meaning that for one path/row location, several land cover maps were produced from images acquired at different times. The land cover maps were integrated mainly by pixel-based majority voting, followed by the adjustment according to the principles of "the greenest" and "the wettest", i.e., vegetation classes have the highest priority on deciding the integrated land cover class (vegetation > water > impervious surfaces > barren lands > snow and ice > clouds). "Clouds" has the lowest priority. It will be filter out if the corresponding pixel is categorized into any land cover type which has higher priority than "Clouds", and be replaced by the majority type of the highest priority as its integrated land cover type. If all images show that this pixel is covered by clouds, it will be kept in the final results, shown as "unidentified" in the integrated map, accounting for a very small percentage of the map.

We consider that the integrated land cover map has lower uncertainty than the individual map produced by a single image acquired at a particular time. To get the seasonal dynamic land cover maps, majority voting and stacking of the individual maps for each season was corrected by the logical inference from the integrated land cover map. In Fig. 8, the logical rules to decide whether the seasonal land cover class should be replaced by the integrated class or kept in its original seasonal class or assigned a modified seasonal class are presented. The vertical axis represents the land cover class on the integrated map, while the horizontal axis represents the land cover class on the map of a single season for the same location. Uncertainty maps are also generated for all seasonal maps using the coding system shown by the circled numbers in Fig. 8, following the rule that the smaller the number, the lower the uncertainty of the seasonal map. For example, the integrated map shows 1 pixel is shrublands, but the majority voting result for this pixel in summer is barren, then it should be withered shrublands. The land cover change affected by life cycle of vegetation and seasonal fluctuations of water supply was depicted by these seasonal dynamic land cover maps.

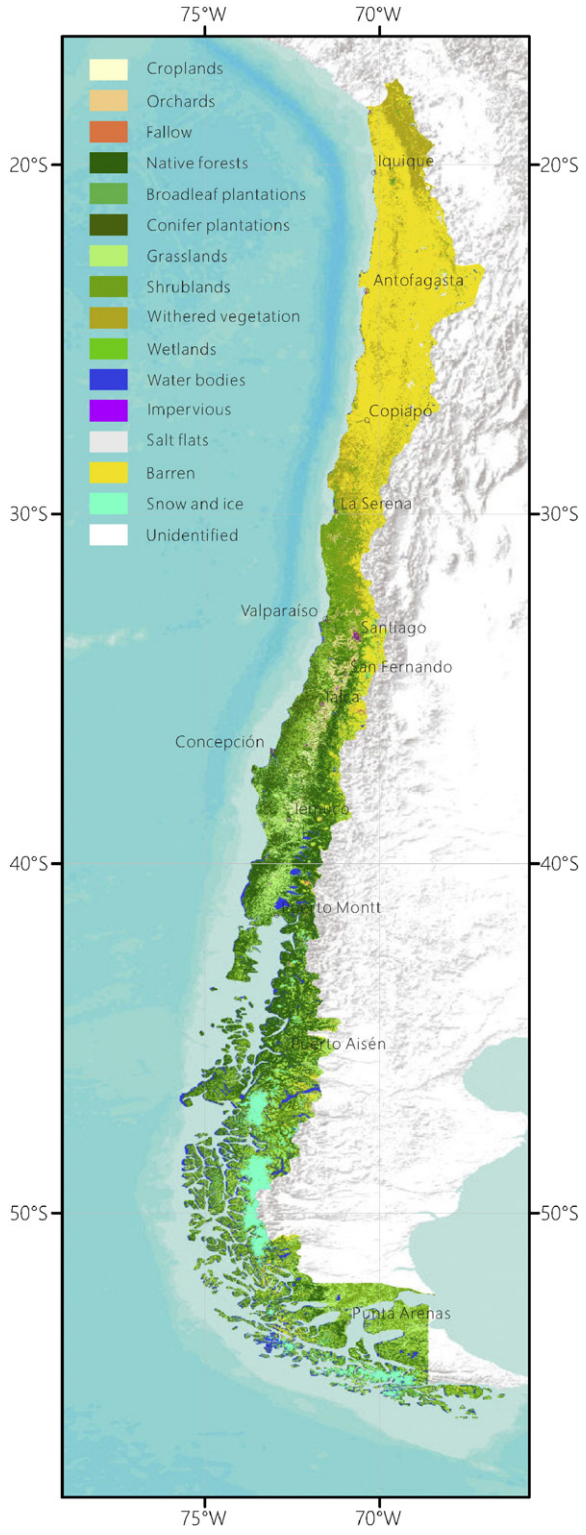

Fig. 9. The integrated land cover map of Chile displayed at the level 1 (plus some level 2 classes) generalization.

3. Results and discussions

3.1. Products and validation

An integrated land cover map for circa 2014 at 30 m spatial resolution was generated for all three levels in the classification scheme. To display it better, the map is shown primarily at level 1, with some

Table 3
Confusion matrix for the integrated Chilean land cover map presented at level 1 (the bold data in the table represents the number of points for which the predicted label is equal to the reference label).

Predicted	Reference									
	Crop	Forests	Grass	Shrub	Water	Impervious	Barren	Snow	Clouds	UA (%)
Croplands	**50**	4	9	1	0	1	0	0	0	77
Forests	2	**324**	5	20	2	0	0	0	0	92
Grasslands	5	11	**184**	33	1	0	0	0	0	79
Shrublands	8	50	59	**257**	4	1	92	0	0	54
Water	0	1	1	0	**50**	0	5	0	0	88
Impervious	0	0	0	0	0	**8**	3	0	0	73
Barren	0	0	6	10	0	4	**441**	1	0	95
Snow/ice	0	0	2	0	0	0	3	**29**	0	85
Clouds	0	0	0	0	0	0	0	1	**0**	0
PA (%)	77	83	69	80	88	57	81	94	–	80

level 2 classes like natural forests, plantations, fallow and withered vegetation in Fig. 9. Accuracy assessment for this map was performed and the overall accuracy is 80% based on an independent validation dataset containing 1688 sample sites well-distributed in the whole country. From the confusion matrix of the map presented at level 1 (Table 3), we could find that all classes were classified with acceptable accuracies. Forests and barren lands have the top users accuracies among all classes, which are 92% and 95%, respectively. Croplands, grasslands, water, snow and ice are classified with users accuracies around or higher than 80%. Snow and ice have the best producers accuracy which is 94%, followed by forests and barren bands. Shrublands have relatively high producers accuracy, but the users accuracy is quite low. Some classified shrublands are actually barren lands. This confusion is caused by the fact that many shrublands in the training sample are comprised of cactus and dry bushes whose spectral profiles are similar to barren lands. The impervious surface is the worst classified class, with quite high omission error, because the urban areas are usually mixed pixels of paved surfaces and vegetation. In addition, the impervious surfaces sometimes look spectrally similar to barren lands.

The overall accuracy for level 2 classes is 73%. Among the subclasses, herbaceous croplands (83% for users accuracy and 74% for producers accuracy), native forests (85% for users accuracy and 76% for producers accuracy), conifer plantations (88% for users accuracy and 77% for producers accuracy), marshlands (76% for users accuracy and 76% for producers accuracy), sandy and rock areas (94% for users accuracy and 80% for producers accuracy) had good classification performance. The level 2 maps for these classes are useful for many applications such as biodiversity conservation, plantation management, and agriculture planning and yield estimation. The accuracies for orchards, broadleaf plantations, pastures, natural grasslands are ranging from 60% to 70%. However, subclasses of shrublands are poorly classified, with the users accuracies varying from 38% to 49% and the producers from 14% to

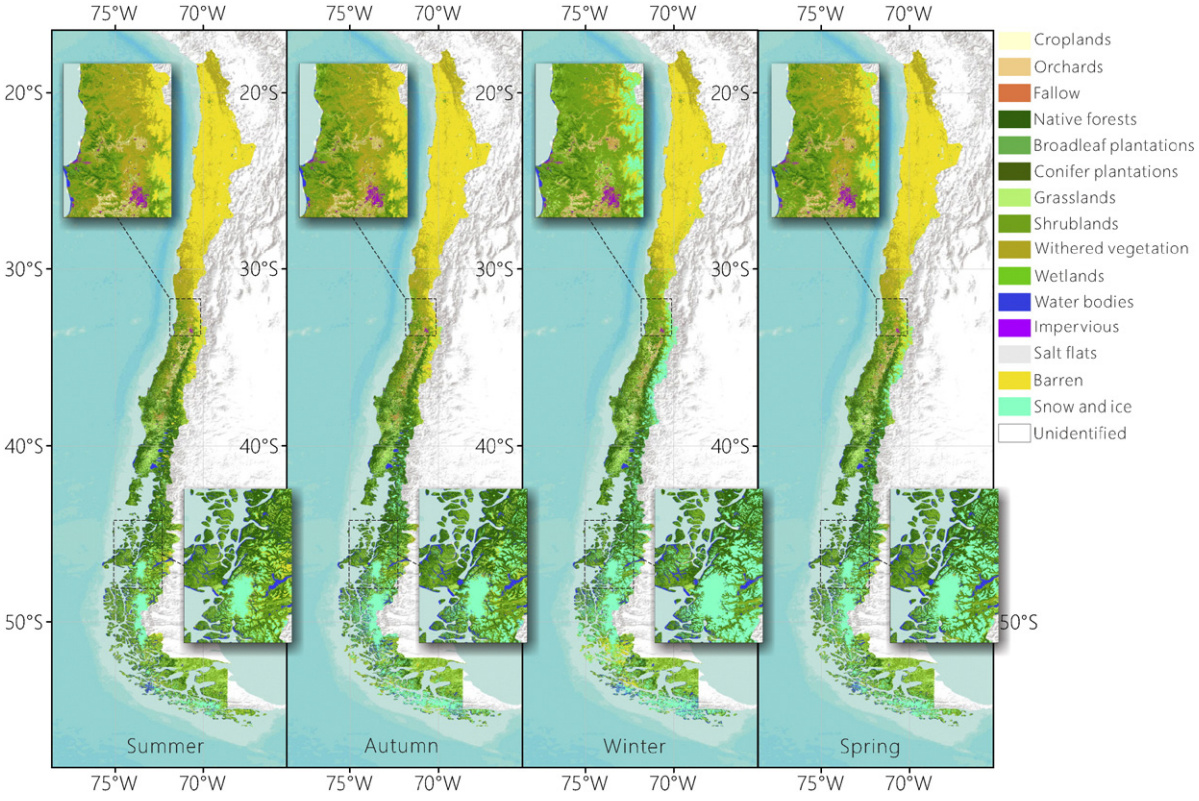

Fig. 10. The seasonal land cover map series of Chile displayed at the level 1 (plus some level 2 classes) generalization.

Table 4
Overall accuracies for seasonal land cover maps at different levels.

Product level	Summer (%)	Autumn (%)	Winter (%)	Spring (%)	Integrated (%)
Level 1 corrected	70	70	69	69	80
Level 1 original	49	49	68	47	
Level 2 corrected	65	64	64	64	73
Level 2 original	43	44	63	43	
Level 3 corrected	53	53	54	53	59
Level 3 original	34	34	53	36	

79%. Shrubs and sparse trees mosaic were the worst, highly confused with secondary native forests.

Seasonal land cover dynamics were reflected in the seasonal maps (Fig. 10). Phenological change of grasses and shrubs, alternation of farming and fallow, variation of water surface, accumulating and melting of snow cover can all be seen on the seasonal maps. The enlarged map on the upper left corner of Fig. 10 shows the area in Valparaíso Region and Santiago Metropolitan Region with a Mediterranean climate. It is obvious to see the greening up of natural vegetation from summer to winter and its withering up from winter to summer. The seasonal land cover map series of the north end of the Patagonian Icefield were enlarged and shown on the lower right corner of each map in Fig. 10, presenting the seasonal expanding and shrinking of snow cover. Since for each validation sample site, dynamic land cover type for each DOY was recorded, the seasonal land cover maps can be validated using the validation dataset. The overall accuracies for the seasonal land cover maps at different level are shown in Table 4, for maps before and after correction according to the integrated map. The overall accuracies for the integrated map are higher than the land cover maps for each season, and much higher than the seasonal maps without the correction. Due to the fact that a large proportion of the country has a Mediterranean climate with wet season in the winter, the accuracies of the original seasonal map from winter images were higher than other seasons without the correction. This proves that images acquired in the growing season of vegetation are superior for land cover mapping.

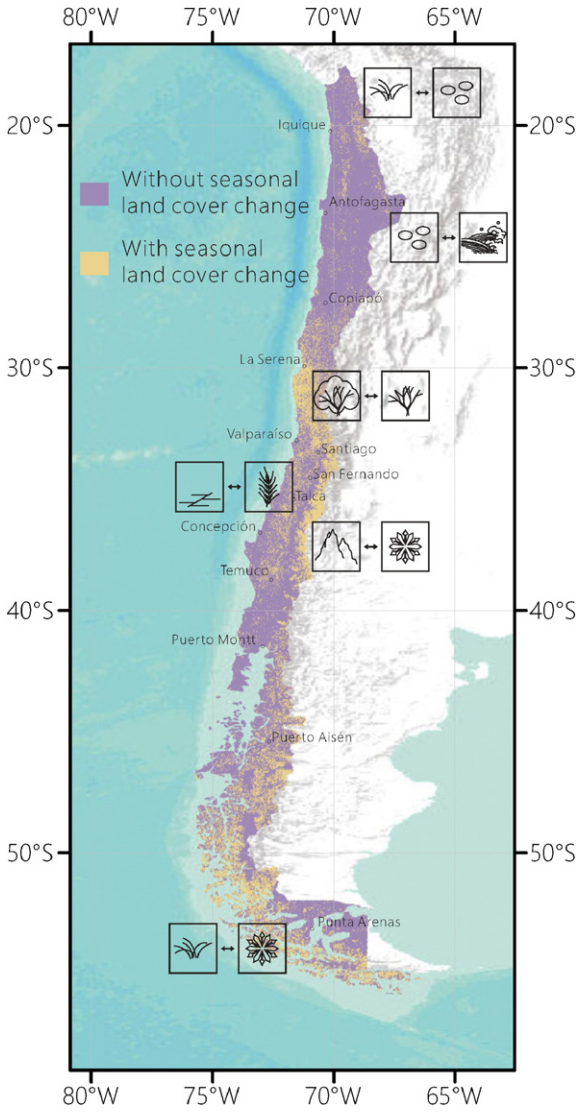

Fig. 11. Distribution of area with seasonal land cover change and the major type of seasonal change.

Our result shows the distribution of areas with seasonal land cover change (see Fig. 11), which accounts for 26.37% of the total area. The major type of seasonal land cover change varies spatially. In the north, seasonal change is mainly the sprouting of vegetation in one season from the barren deserts of other seasons. Another important type of seasonal change in the north is the alternation of salt lakes in summer and salt flats or dry sands for other seasons. In central Chile, seasonal change is mainly shrublands and withered shrublands determined by the winter rainy season of a Mediterranean climate. The southern portion of central Chile has a dominant type of seasonal change from croplands to bare croplands. On the Andes, the main seasonal change comes from the snow cover in winter, as well as the wet south.

3.2. Highlights of thematic contents

The high spatial resolution and the detailed classification scheme of our Chilean land cover products enable users to identify many thematic contents for their own applications. Some representative examples are given below.

One of the most typical and important landscapes in Chile is orchards, which have been well-identified in our maps. Since the 1990s, people have been seeking for potential viticulture area outside the Chilean Central Valley. Due to the high evapotranspiration caused by the abundant sunshine and limited precipitation, they developed their agriculture along the rivers that run down from the Andes Mountains. Fig. 12 shows an example of orchards along one of the most important rivers, the Elqui River in the Region of Coquimbo. From the land cover map in Fig. 12, the impervious surfaces on the upper left corner is La Serena on ocean terraces. Orchards in this area extend from the Pacific coast eastward to the Andes Mountains along the Elqui valley, where people have access to water for irrigation to produce high-quality wine grapes, table grapes and other fruits. Since the area is at the southern end of the Atacama Desert, we can see shrublands and dry rocky terrain surrounding the river valley. The zoomed-in maps of two areas in the dashed boxes are shown with higher resolution DigitalGlobe images. On the left, it is clear to see that the orchards were separated from the herbaceous croplands. The orchards climb up to higher altitudes along the

river valley. From the location presented on the right, the orchard valley narrows down to the east showing the advantage of the 30 m spatial resolution for mapping these features. Field photos taken near this area are presented in Fig. 12.

Wetlands on the high altitude of the Andean mountains, supplied mainly by the outcrops of groundwater, melting glaciers, and lowland accumulated precipitation, are distinctive ecosystems in the arid highlands, locally known as "Bofedales", which is still poorly understood. These wetlands provide special natural habitats for wildlife and are vulnerable to climate change. Our land cover maps provide accurate and dynamic spatial information about the wetlands, the lakes and the salt flats. Fig. 13 shows the map and field photos for part of the Nevado Tres Cruces National Park located in the Atacama Region. On the huge salt flat, referred to as "Salar de Maricunga", shown in the center of the map, we can see the lagoons and wetlands. With the help of seasonal land cover maps on the upper right corner in Fig. 13, seasonal variation of the lagoon water surface and the phenological change of the vegetation can be identified. The lagoons and wetlands are extremely important for many wildlife species. For example, the Andean flamingos shown on the field photos taken in this area, reside in such salt lakes and wetlands during the summer, and migrate to the lower wetlands in the winter. They are one of the rarest flamingos in the world and vulnerable to habitat change.

Native forests and plantations were also differentiated reasonably well. This separation is important as it can provide information for native forest conservation and plantation management. Fig. 14 shows an example near the border of the Bío-Bío Region and the Araucanía Region. This region covers the coastal range dominated by plantations on the west and the central valley dominated by croplands and pastures on the east. The zoomed-in map on the left demonstrates the discrimination of native forests from broadleaf plantations. The plantations dominate on gentle slopes, while native forests only exist in the valley between the slopes. The zoomed-in map on the right is a mix of conifer plantation (left), broadleaf plantation (lower middle) and secondary native forests (right), and they are all mapped correctly. Field photos presented here are pine plantations (left) and eucalyptus plantations (right), mixed with some shrubs and short native forests.

3.3. Spatial variation of accuracy

Information on the spatial variation in accuracy is important because it can indicate regions where more efforts should be spent on land cover map improvements. The overall accuracies were calculated for the WWF ecoregions. Fig. 15 shows the spatial variation of accuracies for level 1 classes, and similar patterns are found for level 2 and level 3 classes. The results indicate the overall accuracy decreases gradually from central Chile to both the north and the south.

The highest local accuracy is in the ecoregion of Chilean Matorral (83.4% at level 1), characterized by a Mediterranean climate. From the very north part of this ecoregion to the immediate south of La Serana is a semi-desert area called "Norte Chico" covered mainly by barren lands, withered shrublands, shrublands and some croplands especially orchards. The Mediterranean center starts from the immediate south of La Serana to the south of the central valley, dominated by shrublands and some sclerophyll forests on moist seaward slopes as natural vegetation, and croplands as well as grassland in the central valley as a result of human activities. The class of shrublands occupies the biggest area in this ecoregion, which is well-classified with a producers accuracy of 87% and a user's accuracy of 75%.

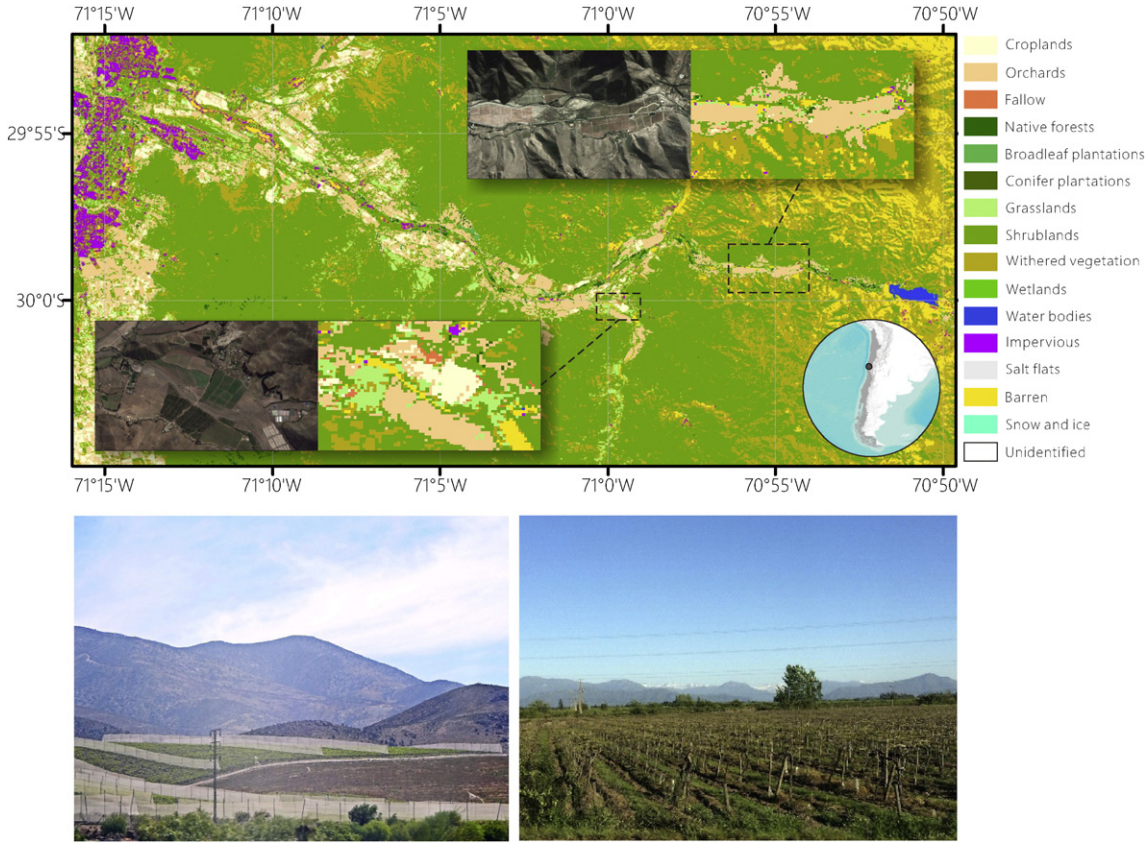

Fig. 12. Mapping result and field photos of the orchards along the Elqui Valley.

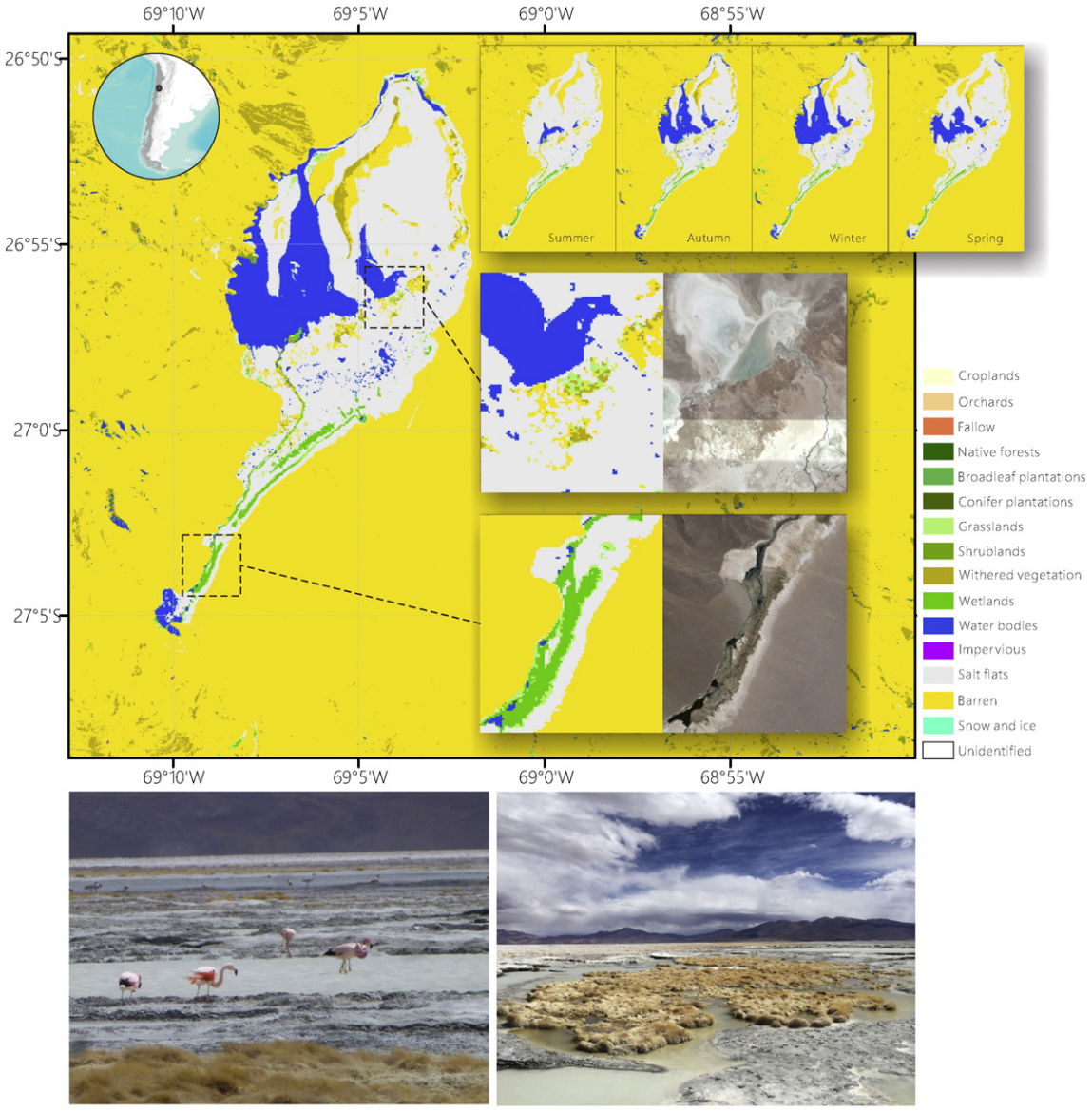

Fig. 13. Dynamic land cover maps and field photos of the wetlands and salt flats near Salar de Maricunga.

The land cover map is also more accurate (83.3% for level 1) for the ecoregion of southern Andean steppe, with an altitudinal zonation of grasslands, shrublands, withered vegetation and barren lands. The barren lands and grasslands were classified with better performance (85.3% and 100% for producers accuracy, 98.3% and 87.5% for users accuracy, respectively), but shrublands are poorly classified. The large proportion of barren lands in this ecoregion raised the overall accuracy.

The overall accuracy for the ecoregion of Valdivian temperate forests at level 1 is 82.9%. The dominant land cover type is forests, which are mainly plantations along the coastal range and native forests on the Andes Mountains. The native forest and plantations are categorized with producers accuracies of 81.7% and 79.4%, users accuracies of 88.4% and 80.6%. The major land cover type for the central valley is pastures, whose producers accuracy is 73.9% and users accuracy is 59.6%, mainly confused with natural grasslands.

The Central Andean dry puna is a unique ecoregion located in the Andean High plateau, which includes mainly barren lands, dry shrublands and grasslands, and interspersed with some wetlands along the streams. The overall accuracy is 81.4% at level 1, but the dry shrublands are confused with barren lands in this ecoregion, due to their similar spectral characteristics. Some salt flats were categorized into gravels which is also a major confusion. The wetlands of this area are well-identified whose producers and users accuracies are both higher than 90%.

The Atacama Desert has a lower accuracy (80.3% at level 1) because the validation dataset did not sample enough in the vast desert completely devoid of life. There are only 51 sample units in this region, and there is a confusion between barren lands and withered shrublands.

The Magellanic subpolar forests and Patagonian steppe have the lowest accuracies of 64.8% and 66.7%, respectively. This is due to lack of cloud free images over these regions. In these regions, forests are short resulting in more confusion with shrublands.

4. Conclusions and perspectives

A 30 m spatial resolution Chilean land cover map and a seasonal land cover map series were produced for circa 2014 primarily using Landsat 8 imagery. The classification scheme is more detailed than existing land cover databases. The classes derived in this study are able to support more applications in biodiversity conservation, land surface modelling, resource management and planning. This is the first nationwide land cover map for Chile through close international collaboration between

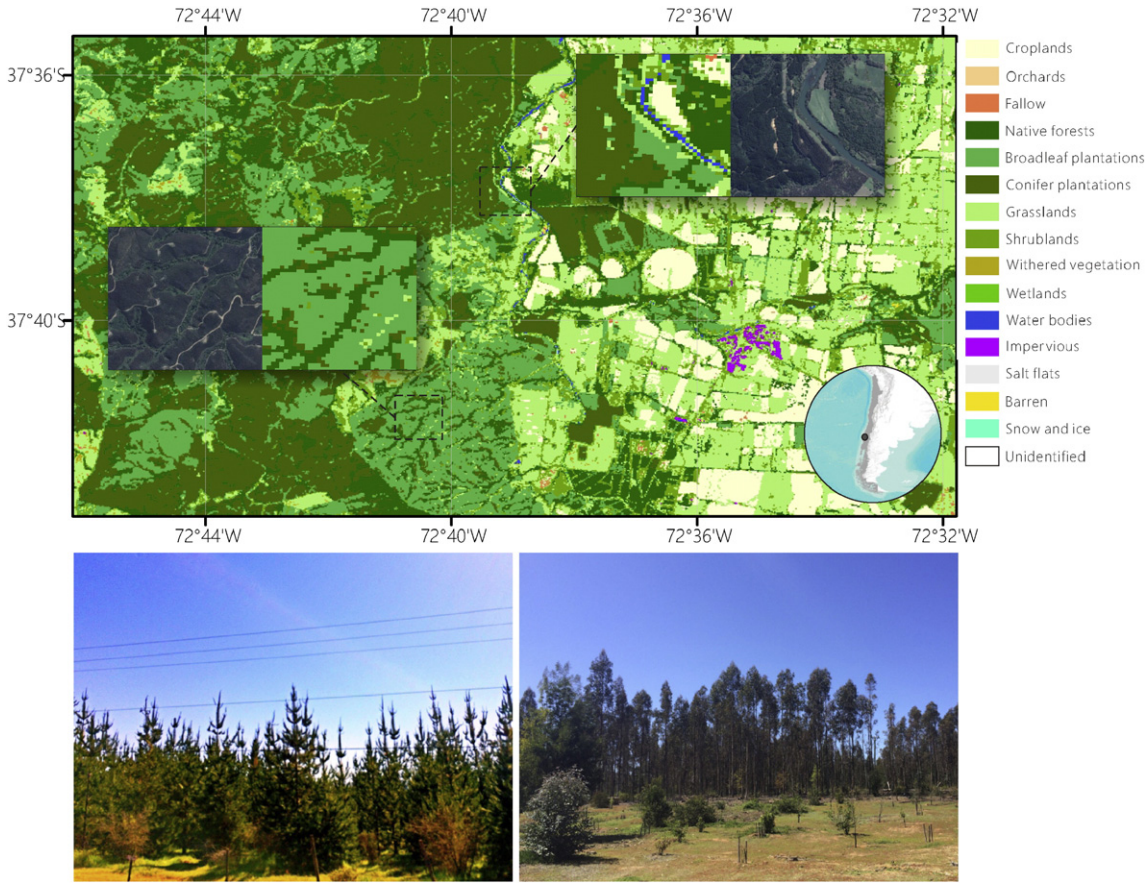

Fig. 14. Mapping result and field photos of the native forests and plantations in Bío-Bío Region.

local experts and researchers in China and the US. Field works by the international team helped improving the scheme design, training sample interpretation and validation. The overall accuracy reached 80% for level 1 product and 73% for level 2 thanks to the integration of multi-seasonal data. This study is among the first ones that generate seasonal land cover dynamics. Our previous dynamics land cover mapping efforts with medium resolution satellite data are restricted to a lake or municipality area (Dronova et al., 2015; Wang et al., 2015). Here we extended this capability to a whole nation. The seasonal land cover maps for Chile are also validated. Through correction according to the integrated map, it is possible to substantially improve accuracies of seasonal land cover maps. The analysis of spatial variation of accuracy among the ecoregions indicates that the accuracy for land cover mapping decreases gradually from central Chile to both north and south, providing useful information for directing future efforts in Chile.

Multi-temporal images play a vital role in improving our mapping process, and they work in three ways together. Experiments showed that mapping accuracies were improved by (1) combining multi-temporal training samples collected from multi-temporal images, (2) adding a four season NDVI series to the feature set, and (3) integrating the classification results of many multi-temporal images.

The accuracy for land cover mapping in Chile could be further improved by the inclusion of additional ancillary data. DMSP Operational Linescan System (OLS) nighttime stable light (NTL) datasets could be used to differentiate the urban area, which is poorly classified in the current map. Since the urban area is always a mosaic of vegetation and impervious surface, training samples of impervious surfaces are usually not pure pixels, leading to serious confusion between impervious surfaces and other land cover types. Though the night light data has lower spatial resolution, it can be used as a mask for potential urban area, i.e. removing training samples of impervious surfaces from the training set outside the mask, while putting more training samples of impervious surfaces inside the mask, and merge these two layer for a final result. In addition, microwave data might be useful over the subpolar areas that are frequently covered by clouds. For example, Advanced Land Observing Satellite (ALOS) Phased Array type L-band Synthetic Aperture Radar (PALSAR) data has been proved effective in some researches (Zhu et al., 2012).

The multi-temporal NDVI series we used now in the feature set is the MVC result, in order to eliminate the disturbance of cloud contamination and keep the feature vector in the same length. Sometimes the MVC result may hide some patterns in the seasonal variation. We can take not only MVC but also other metrics for each season, for example the upper and lower quartiles. Experiments should be designed for feature selection. The integration strategy of multi-seasonal mapping as well as the logic rules for the seasonal map correction could also be further refined. The post-classification strategy in our study is simple and fast, and it can be improved by estimating the probability of all alternatives and analyzing the uncertainty using more statistical methods (McRoberts, 2010; Olofsson et al., 2012; Sexton et al., 2015).

The mapping result reported here is only for 1 year around 2014. Long-term land cover dynamics are important for monitoring land cover changes which can be used in many applications, such as studies on fire disturbance (Carmona, González, Nahuelhual, & Silva, 2012), replacement of native forest by exotic plantations (Little, Lara, McPhee, & Urrutia, 2009), deforestation and habitat change (Echeverria et al., 2006; Vergara, Perez-Hernandez, Hahn, & Soto, 2013). The training dataset includes samples spatially distributed in the whole country, temporally distributed throughout a year, and covering different land cover types. We believe that we have a relatively exhaustive training dataset that could be used to train a universal model for the classification of any image newly acquired for Chile. To produce a long-term

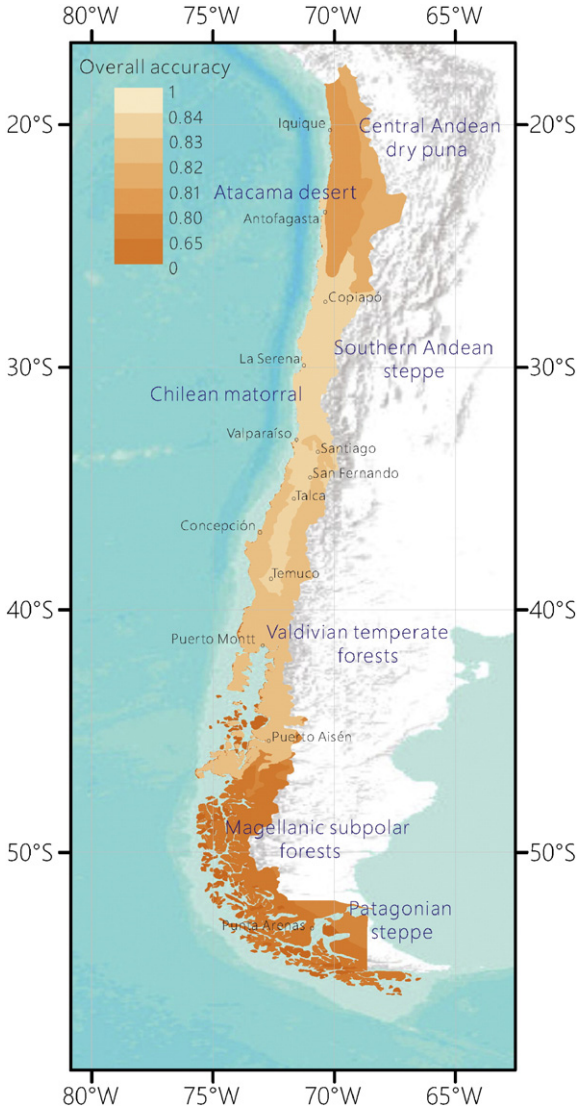

Fig. 15. Spatial variation of overall accuracy among different ecoregions.

dynamic product for the past, images of Landsat 5 Surface Reflectance CDR datasets were also prepared back to the 1980s. We will test the training sample from Landsat 8 images to classify Landsat 5 images following some consistency checks. We expect to produce a historical long-term land cover dynamics multi-seasonal dataset for Chile in the near future. The land cover data presented in this paper will be open access on data.ess.tsinghua.edu.cn.

Acknowledgements

This research is funded by a project (Development of advanced remote sensing methods for mapping and managing plant species diversity in Mediterranean Forests of Chile and California, 2013–2014) in UC Berkeley-Chile Seed Funds (grant number: 77477) and a Meteorological Public Benefit project of China (grant number: GYHY201506010).

References

Altamirano, A., Aplin, P., Miranda, A., Cayuela, L., Algar, A. C., & Field, R. (2013). High rates of forest loss and turnover obscured by classical landscape measures. *Applied Geography*, *40*, 199–211.

Arvor, D., Jonathan, M., Meirelles, M. S. P., Dubreuil, V., & Durieux, L. (2011). Classification of modis evi time series for crop mapping in the state of Mato Grosso, Brazil. *International Journal of Remote Sensing*, *32*, 7847–7871.

Blanco, P. D., Colditz, R. R., Saldaña, G. L., Hardtke, L. A., Llamas, R. M., Mari, N. A., Fischer, A. , Caride, C., Aceñolaza, P. G., Del Valle, H. F., et al. (2013). A land cover map of Latin America and the Caribbean in the framework of the serena project. *Remote Sensing of Environment*, *132*, 13–31.

Brisco, B., & Brown, R. (1995). Multidate sar/tm synergism for crop classification in western Canada. *Photogrammetric Engineering and Remote Sensing*, *61*, 1009–1014.

Carmona, A., González, M. E., Nahuelhual, L., & Silva, J. (2012). Spatio-temporal effects of human drivers on fire danger in Mediterranean Chile. *Bosque*, *33*, 321–328.

Cartwright, D., & Gaston, C. (2002). Chile's forest products markets-a plantation success story. *Forest products annual market review*.

Dai, Y., Zeng, X., Dickinson, R. E., Baker, I., Bonan, G. B., Bosilovich, M. G., Denning, A. S., Dirmeyer, P. A., Houser, P. R., Niu, G., et al. (2003). The common land model. *Bulletin of the American Meteorological Society*, *84*, 1013–1023.

Di Gregorio, A. (2005). *Land cover classification system: Classification concepts and user manual: LCCS. Vol. 8*, Food & Agriculture Org.

Dong, Z., Wang, Z., Liu, D., Song, K., Li, L., Jia, M., & Ding, Z. (2014). Mapping wetland areas using landsat-derived ndvi and lswi: A case study of west Songnen plain, Northeast China. *Journal of the Indian Society of Remote Sensing*, *42*, 569–576.

Dronova, I., Gong, P., Wang, L., & Zhong, L. (2015). Mapping dynamic cover types in a large seasonally flooded wetland using extended principal component analysis and object-based classification. *Remote Sensing of Environment*, *158*, 193–206.

Echeverria, C., Coomes, D., Salas, J., Rey-Benayas, J. M., Lara, A., & Newton, A. (2006). Rapid deforestation and fragmentation of Chilean temperate forests. *Biological Conservation*, *130*, 481–494.

Espinosa, M., Acuña, E., Cancino, J., Muñoz, F., & Perry, D. A. (2005). Carbon sink potential of radiata pine plantations in Chile. *Forestry*, *78*, 11–19.

Eva, H. D., Belward, A. S., De Miranda, E. E., Di Bella, C. M., Gond, V., Huber, O., ... Fritz, S. (2004). A land cover map of South America. *Global Change Biology*, *10*, 731–744.

Fagan, M. E., DeFries, R. S., Sesnie, S. E., Arroyo-Mora, J. P., Soto, C., Singh, A., ... Chazdon, R. L. (2015). Mapping species composition of forests and tree plantations in northeastern Costa Rica with an integration of hyperspectral and multitemporal landsat imagery. *Remote Sensing*, *7*, 5660–5696.

Friedl, M. A., Sulla-Menashe, D., Tan, B., Schneider, A., Ramankutty, N., Sibley, A., & Huang, X. (2010). Modis collection 5 global land cover: Algorithm refinements and characterization of new datasets. *Remote Sensing of Environment*, *114*, 168–182.

Giri, C., & Long, J. (2014). Land cover characterization and mapping of South America for the year 2010 using landsat 30 m satellite data. *Remote Sensing*, *6*, 9494–9510.

Gong, P. (2012). Remote sensing of environmental change over China: A review. *Chinese Science Bulletin*, *57*, 2793–2801.

Gong, P., Wang, J., Yu, L., Zhao, Y., Zhao, Y., Liang, L., Niu, Z., Huang, X., Fu, H., Liu, S., et al. (2013). Finer resolution observation and monitoring of global land cover: First mapping results with landsat tm and etm + data. *International Journal of Remote Sensing*, *34*, 2607–2654.

Guerschman, J., Paruelo, J., Bella, C. D., Giallorenzi, M., & Pacin, F. (2003). Land cover classification in the argentine pampas using multi-temporal landsat tm data. *International Journal of Remote Sensing*, *24*, 3381–3402.

Hansen, M., DeFries, R., Townshend, J. R., & Sohlberg, R. (2000). Global land cover classification at 1 km spatial resolution using a classification tree approach. *International Journal of Remote Sensing*, *21*, 1331–1364.

Henebry, G. M. (1993). Detecting change in grasslands using measures of spatial dependence with landsat tm data. *Remote Sensing of Environment*, *46*, 223–234.

Hess, L. L., Melack, J. M., Novo, E. M., Barbosa, C. C., & Gastil, M. (2003). Dual-season mapping of wetland inundation and vegetation for the central amazon basin. *Remote Sensing of Environment*, *87*, 404–428.

Hojas Gascon, L., Eva, H., Gobron, N., Simonetti, D., & Fritz, S. (2012). The application of medium-resolution meris satellite data for continental land-cover mapping over South America—Results and caveats. *Remote sensing of land use and land cover: Principles and applications*. Boca Raton, Fl: CRC/Taylor & Francis.

Holben, B. N. (1986). Characteristics of maximum-value composite images from temporal avhrr data. *International Journal of Remote Sensing*, *7*, 1417–1434.

Homer, C., Dewitz, J., Fry, J., Coan, M., Hossain, N., Larson, C., ... Wickham, J. (2007). Completion of the 2001 national land cover database for the counterminous United States. *Photogrammetric Engineering and Remote Sensing*, *73*, 337.

Jung, M., Henkel, K., Herold, M., & Churkina, G. (2006). Exploiting synergies of global land cover products for carbon cycle modeling. *Remote Sensing of Environment*, *101*, 534–553.

LaFontaine, J. H., Hay, L. E., Viger, R. J., Regan, R. S., & Markstrom, S. L. (2015). Effects of climate and land cover on hydrology in the Southeastern US: Potential impacts on watershed planning. *JAWRA Journal of the American Water Resources Association*.

Lanfranco, D., & Dungey, H. (2001). Insect damage in eucalyptus: A review of plantations in Chile. *Austral Ecology*, *26*, 477–481.

Liang, L., Xu, B., Chen, Y., Liu, Y., Cao, W., Fang, L., ... Li, W. (2010). Combining spatial-temporal and phylogenetic analysis approaches for improved understanding on global h5n1 transmission. *PloS One*, *5*, e13575.

Little, C., Lara, A., McPhee, J., & Urrutia, R. (2009). Revealing the impact of forest exotic plantations on water yield in large scale watersheds in south-central Chile. *Journal of Hydrology*, *374*, 162–170.

Liu, J., Chen, J., Cihlar, J., & Park, W. (1997). A process-based boreal ecosystem productivity simulator using remote sensing inputs. *Remote Sensing of Environment*, *62*, 158–175.

Lo, T. H., Scarpace, F. L., & Lillesand, T. M. (1986). Use of multitemporal spectral profiles in agricultural land-cover classification. *Photogrammetric Engineering and Remote Sensing (USA)*.

McRoberts, R. E. (2010). Probability- and model-based approaches to inference for proportion forest using satellite imagery as ancillary data. *Remote Sensing of Environment*, *114*, 1017–1025.
Moreira-Muñoz, A. (2011). *Plant geography of Chile. vol. 5*, Springer Science & Business Media.
Munro, D., & Touron, H. (1997). The estimation of marshland degradation in southern Iraq using multitemporal landsat tm images. *International Journal of Remote Sensing*, *18*, 1597–1606.
Nahuelhual, L., Carmona, A., Lara, A., Echeverra, C., & González, M. E. (2012). Land-cover change to forest plantations: Proximate causes and implications for the landscape in south-central Chile. *Landscape and Urban Planning*, *107*, 12–20.
Olofsson, P., Stehman, S. V., Woodcock, C. E., Sulla-Menashe, D., Sibley, A. M., Newell, J. D., ... Herold, M. (2012). A global land-cover validation data set, part i: Fundamental design principles. *International Journal of Remote Sensing*, *33*, 5768–5788.
Özesmi, U., & Mitsch, W. J. (1997). A spatial habitat model for the marsh-breeding red-winged blackbird (*Agelaius phoeniceus* l.) in coastal Lake Erie wetlands. *Ecological Modelling*, *101*, 139–152.
Panayotou, T., & Ashton, P. (1992). *Not by timber alone: Economics and ecology for sustaining tropical forests*. Island Press.
Pauleit, S., & Duhme, F. (2000). Assessing the environmental performance of land cover types for urban planning. *Landscape and Urban Planning*, *52*, 1–20.
Pearson, R. G., Dawson, T. P., & Liu, C. (2004). Modelling species distributions in Britain: A hierarchical integration of climate and land-cover data. *Ecography*, *27*, 285–298.
Peña, M., & Brenning, A. (2015). Assessing fruit-tree crop classification from landsat-8 time series for the Maipo valley, Chile. *Remote Sensing of Environment*, *171*, 234–244.
Potapov, P., Turubanova, S., Tyukavina, A., Krylov, A., McCarty, J., Radeloff, V., & Hansen, M. (2015). Eastern Europe's forest cover dynamics from 1985 to 2012 quantified from the full landsat archive. *Remote Sensing of Environment*, *159*, 28–43.
Schriever, J. R., & Congalton, R. G. (1995). Evaluating seasonal variability as an aid to cover-type mapping from landsat thematic mapper data in the northeast. *Photogrammetric Engineering and Remote Sensing*, *61*, 321–327.
Schulz, J. J., Cayuela, L., Echeverria, C., Salas, J., & Benayas, J. M. R. (2010). Monitoring land cover change of the dryland forest landscape of central Chile (1975–2008). *Applied Geography*, *30*, 436–447.
Senf, C., Leitão, P. J., Pflugmacher, D., van der Linden, S., & Hostert, P. (2015). Mapping land cover in complex mediterranean landscapes using landsat: Improved classification accuracies from integrating multi-seasonal and synthetic imagery. *Remote Sensing of Environment*, *156*, 527–536.
Sexton, J. O., Noojipady, P., Anand, A., Song, X. -P., McMahon, S., Huang, C., ... Townshend, J. R. (2015). A model for the propagation of uncertainty from continuous estimates of tree cover to categorical forest cover and change. *Remote Sensing of Environment*, *156*, 418–425.
Squeo, F. A., Estévez, R. A., Stoll, A., Gaymer, C. F., Letelier, L., & Sierralta, L. (2012). Towards the creation of an integrated system of protected areas in Chile: Achievements and challenges. *Plant Ecology & Diversity*, *5*, 233–243.
Stone, T. A., Schlesinger, P., Houghton, R. A., & Woodwell, G. M. (1994). Map of the vegetation of South America based on satellite imagery. *Photogrammetric Engineering and Remote Sensing*, *60*.
Sun, F., Zhao, Y., Gong, P., Ma, R., & Dai, Y. (2014). Monitoring dynamic changes of global land cover types: Fluctuations of major lakes in China every 8 days during 2000–2010. *Chinese Science Bulletin*, *59*, 171–189.
Toro, J., & Gessel, S. (1999). Radiata pine plantations in Chile. In J. Boyle, J. Winjum, K. Kavanagh, & E. Jensen (Eds.), *Planted forests: Contributions to the quest for sustainable societies. Of Forestry Sciences*, *Vol. 56*. (pp. 393–404). Springer Netherlands (URL: http://dx.doi.org/10.1007/978-94-017-2689-4_25 . doi: 10.1007/978–94–017-2689-4_25).
Townshend, J. R., Justice, C., & Kalb, V. (1987). Characterization and classification of South American land cover types using satellite data. *International Journal of Remote Sensing*, *8*, 1189–1207.
Tucker, C. J., Townshend, J. R., & Goff, T. E. (1985). African land-cover classification using satellite data. *Science*, *227*, 369–375.
Vergara, P. M., Perez-Hernandez, C. G., Hahn, I. J., & Soto, G. E. (2013). Deforestation in central Chile causes a rapid decline in landscape connectivity for a forest specialist bird species. *Ecological Research*, *28*, 481–492.
Wang, J., Zhao, Y., Li, C., Yu, L., Liu, D., & Gong, P. (2015). Mapping global land cover in 2001 and 2010 with spatial-temporal consistency at 250 m resolution. *ISPRS Journal of Photogrammetry and Remote Sensing*, *103*, 38–47.
Wolter, P. T., Mladenoff, D. J., Host, G. E., & Crow, T. R. (1995). Improved forest classification in the northern lake states using multi-temporal landsat imagery. *Photogrammetric Engineering and Remote Sensing*, *61*, 1129–1144.
Yang, J., Gong, P., Fu, R., Zhang, M., Chen, J., Liang, S., ... Dickinson, R. (2013). The role of satellite remote sensing in climate change studies. *Nature Climate Change*, *3*, 875–883.
Yu, L., Liang, L., Wang, J., Zhao, Y., Cheng, Q., Hu, L., ... Gong, P. (2014a). Meta-discoveries from a synthesis of satellite-based land-cover mapping research. *International Journal of Remote Sensing*, *35*, 4573–4588. http://dx.doi.org/10.1080/01431161.2014.930206 (URL: http://www.tandfonline.com/doi/abs/10.1080/01431161.2014.930206).
Yu, L., Shi, Y., & Gong, P. (2015). Land cover mapping and data availability in critical terrestrial ecoregions: A global perspective with landsat thematic mapper and enhanced thematic mapper plus data. *Biological Conservation*, *190*, 34–42.
Yu, L., Wang, J., Li, X., Li, C., Zhao, Y., & Gong, P. (2014b). A multi-resolution global land cover dataset through multisource data aggregation. *Science China Earth Sciences*, *57*, 2317–2329.
Zhao, Y., Gong, P., Yu, L., Hu, L., Li, X., Li, C., Zhang, H., Zheng, Y., Wang, J., Zhao, Y., et al. (2014). Towards a common validation sample set for global land-cover mapping. *International Journal of Remote Sensing*, *35*, 4795–4814.
Zhong, L., Gong, P., & Biging, G. S. (2012). Phenology-based crop classification algorithm and its implications on agricultural water use assessments in California's central valley. *Photogrammetric Engineering & Remote Sensing*, *78*, 799–813.
Zhong, L., Gong, P., & Biging, G. S. (2014). Efficient corn and soybean mapping with temporal extendability: A multi-year experiment using landsat imagery. *Remote Sensing of Environment*, *140*, 1–13.
Zhu, Z., Woodcock, C. E., Rogan, J., & Kellndorfer, J. (2012). Assessment of spectral, polarimetric, temporal, and spatial dimensions for urban and peri-urban land cover classification using landsat and sar data. *Remote Sensing of Environment*, *117*, 72–82.